

## Durability of steel fiber reinforced self-compacting concrete



Cristina Frazão<sup>a,\*</sup>, Aires Camões<sup>b</sup>, Joaquim Barros<sup>a</sup>, Delfina Gonçalves<sup>c</sup>

<sup>a</sup> ISISE, Dept. of Civil Engineering, University of Minho, Campus de Azurém, Guimarães, Portugal

<sup>b</sup> CTAC, Dept. of Civil Engineering, University of Minho, Campus de Azurém, Guimarães, Portugal

<sup>c</sup> CiviTest, 4770-160 Jesufrei, Vila Nova de Famalicão, Portugal

### HIGHLIGHTS

- Mechanical properties and durability indicators of SFRSCC and SCC were assessed.
- Self-compacting requisites were maintained, adding 60 kg/m<sup>3</sup> of steel fibers to SCC.
- Steel fibers contributed for the increase of post-cracking flexural resistance.
- The addition of steel fibers to SCC did not affect the durability indicators.

### ARTICLE INFO

#### Article history:

Received 7 November 2014

Received in revised form 6 January 2015

Accepted 12 January 2015

Available online 9 February 2015

#### Keywords:

Durability

SFRSCC

Corrosion

Electrical resistivity

Chloride penetration

Carbonation

### ABSTRACT

Durability is one of the most important aspects of concrete due to its fundamental incidence on the serviceability working conditions of concrete structures. Research on the durability of steel fiber reinforced self-compacting concrete (SFRSCC) is still scarce, particularly in the aspects of corrosion resistance, which did not yet demonstrate clearly whether the corrosion of steel fibers may or may not lead to cracking and subsequent spalling of the surrounding concrete.

For conventional concrete, without steel fibers, there are some widespread used durability indicators, which applicability to SFRSCC and its common values are practically unknown. For this purpose, an experimental work with SFRSCC and self-compacting concrete (SCC) specimens was carried out in order to characterize their mechanical properties and evaluate durability indicators.

The results showed that the addition of steel fibers to SCC was very effective in terms of increasing the post-cracking flexural resistance and the energy absorption, and did not affect significantly the self-compacting requisites and the durability indicators of SCC.

© 2015 Elsevier Ltd. All rights reserved.

### 1. Introduction

Steel fibers have been successfully used in concrete to improve its mechanical properties, such as post-cracking load bearing capacity and energy absorption performance. Fibers are also used to limit the crack width, with beneficial consequences in terms of concrete durability. An increase in the crack width promotes the concrete permeability, favoring the occurrence of corrosion of steel reinforcements [1,20,34]. In this context, steel fibers are presented as a solution for this problem, since due to fiber reinforcement mechanisms, the maximum crack width can be limited,

and the concrete ductility and post-cracking resistance can be significantly improved [36]. Material transport properties, especially permeability, may affect the durability and integrity of a structure [37,36]. The increase in concrete permeability, due to the initiation and propagation of cracks, provides ingress of water, chlorides and other corrosive agents, facilitating deterioration [50,32]. At larger crack widths (>100 μm), steel fibers might stitch the cracks, shortening the depth of the crack, and reducing crack area for permeability [37,2]. This is probably due to the crack stitching and multiple cracking effects provided by steel fiber reinforcement that improves resistance to water permeation [37,21,2]. The ability of steel fiber reinforced concrete (SFRC) to transfer tensile forces across cracked sections decreases the crack spacing and increases the tension stiffening, both of which contribute to an improved crack control [6]. For a crack width less than 100 μm, steel fibers do not seem to affect the permeability [37]. The permeability of SFRC decreases significantly by increasing the fiber content and the curing time period [46]. This is mainly attributed to the reduc-

\* Corresponding author.

E-mail addresses: [frazao\\_cristina@hotmail.com](mailto:frazao_cristina@hotmail.com) (C. Frazão), [aires@civil.uminho.pt](mailto:aires@civil.uminho.pt) (A. Camões), [barros@civil.uminho.pt](mailto:barros@civil.uminho.pt) (J. Barros), [delfinagoncalves@civitest.com](mailto:delfinagoncalves@civitest.com) (D. Gonçalves).

URLs: <http://www.isise.net> (C. Frazão), <http://www.ctac.uminho.pt> (A. Camões), <http://www.isise.net> (J. Barros), <http://www.civitest.pt> (D. Gonçalves).

tion of shrinkage cracks, and due to the breaking of the continuity of pores and inter-connectivity of porous channels by the fiber reinforcement mechanisms [46]. If the concrete is less permeable, the detrimental substances, such as chloride ion, sulfate ion and acid, cannot easily penetrate into the concrete, and thus the durability of structure is better preserved [44].

In self-compacting cementitious composites, the investigation of several durability indicators, such as mercury porosity, oxygen permeability, chloride diffusion and chloride migration showed that minor alterations were introduced by the addition of fibers [43,41,48]. The interfacial zone around the fibers does not act as a preferential path for penetration of detrimental agents [48]. Based on published research regarding the durability properties of SFRC, it is argued that steel fibers could be used in reinforced concrete structures exposed to chloride environments to improve their overall durability performance [5]. However, further experimental results for supporting this hypothesis are needed, particularly on corrosion resistance, which was not yet fully addressed, for example, whether the corrosion of the fibers may, or may not, lead to cracking and subsequent spalling of the surrounding concrete.

Since durability is a major topic in concrete structures nowadays, and considering that the use of steel fiber reinforced self-compacting concrete (SFRSCC) is progressively growing in the field of structural elements, there is now an increasing need of a better understanding of SFRSCC behavior in response to environmental actions. Thus, the need to obtain durability indicators is of paramount importance for a larger acceptance of this composite material. For this purpose, in this work, some indicators on the durability performance of SFRSCC are compared to those obtained in equivalent SCC. To characterize their performance, SFRSCC and SCC specimens were subjected to ten different types of tests, some of them for the mechanical characterization (elasticity modulus, compressive strength and flexural behavior) and the others for the evaluation of durability indicators normally used to assess the durability performance of conventional concrete, namely: water absorption by immersion and by capillarity, permeability to air, electrical resistivity, chloride diffusion by migration under non-steady state, resistance to chloride penetration by immersion and carbonation. The tests, executed at 28 days, are described and the results are presented and analyzed in this work. Due to a special incidence of this work on the corrosion of the steel fibers, the following chapter is dedicated to a short state-of-the-art on the corrosion of steel fibers for the reinforcement of concrete materials.

## 2. Corrosion resistance of SFRSCC

The corrosion has a detrimental effect on the durability of reinforced concrete structures. The primary causes of corrosion are chloride-penetration, and the reduction of pH of the concrete matrix due to carbonation [1]. Corrosion affects the fibers bridging the cracks with detrimental consequences in terms of the performance of SFRC structures. Corrosion spots appear on the concrete surfaces exposed to adverse environments.

Insufficient knowledge on the deterioration mechanisms caused by fiber corrosion contributes for a conservative design philosophy, which limits the mobilization of the full potential of SFRC [47]. In fact, some design guidelines recommend not taking into account the contribution of fiber reinforcement of a certain layer thickness for the evaluation of the flexural resistance of SFRC members [40].

Corrosive agents, in liquid and gaseous state, may penetrate the concrete through one of the three transport mechanisms: diffusion, capillary absorption and permeation. Permeation is considered to be the dominant mechanism, and is highly dependent on the concrete cracking process. An increase in the crack width not only produces a highly permeable concrete, but also enhances the possibility of fiber corrosion.

It is widely reported that in case of SFRC, steel fiber corrosion is much less severe as compared with steel rebar reinforcement of concrete structures [3]. Due to large surface area to volume ratio, steel fibers are more effectively screened by the lime rich layer than the large diameter bars used in conventional reinforced concrete. However, the corrosion of fibers can produce micro-spalling of concrete, as well as the reduction of the sectional area of the fibers, which fact causes concern on the long term material and structural performances of SFRC structures [20].

The corrosion resistance of SFRC is governed by the same factors that influence the corrosion resistance of conventionally reinforced concrete. Processes such as carbonation, penetration of chloride ions and sulphate attack are related to the permeability of the cement matrix. As long as the matrix retains its inherent alkalinity and remains uncracked, deterioration of SFRC is not likely to occur. Saojeng and Weiting [44] carried out an accelerated corrosion test in SFRC specimens to evaluate chloride permeability and corrosion behavior. For corrosion test, a 12.7 mm-diameter rebar was embedded in the center of the cylindrical SFRC specimens, leaving an exposed length of 100 mm in 3.5% NaCl solution (controlled by epoxy-seal application). The corrosion cell was connected so that the rebar acted as working electrode, saturated calomel electrode as reference electrode, and the titanium mesh as counter electrode. A current density of 0.5 mA/cm<sup>2</sup> was applied and the open circuit potential (OCP) and linear polarization resistance were measured using a potentiostat. The duration of the corrosion test was selected as 480 h. During this test, it was observed that by increasing the steel fiber content, both the OCP and the polarization resistance have increased, the first one slightly, while the second one significantly. Little corrosion products were found on the rebar and steel fibers. Corrosion was almost restricted to the fibers at the surface, since the fibers embedded in the internal cement-based composite were preserved free of corrosion.

Carbonation penetration rate is determined by the permeability of the concrete and decreases with time, which means that the process is self-decelerating. Carbonation starts at the concrete surface and continues inwards, as long as there is enough carbon dioxide available. In practice it has been found that the carbonation front is stopped when it reaches the large supply of the lime around the fiber. When a fiber loses this protective passivation layer its corrosion process starts, maintaining fibers at deeper position free from corrosion [9]. Steel fibers close to the exposed concrete surface show signs of corrosion due to carbonation of the surrounding concrete, but there is no evidence of concrete spalling due to the carbonation front [9].

The chloride diffusivity depends on the concrete pore structure and all the factors that determine it, such as, mix design parameters (W/C ratio, type and proportion of mineral admixtures and cement, compaction, curing, etc.) and presence of cracks [45]. Literature is mainly focused on corrosion arising from cracking process [20,51,34]. There are three main consequences of corrosion in SFRC associated to the cracking process: (1) a decrease of the carrying capacity and energy absorption performance of the SFRC element (more brittle behavior); (2) due to the rust formation from fiber corrosion process, fiber-paste friction can increase, enhancing the fiber pullout response, with beneficial effects in terms of load carrying capacity and energy absorption of the SFRC element; (3) if the crack width is small enough that self-healing almost restores SFRC integrity, fiber corrosion has negligible influence in terms of structural and durability performance [20]. The first consequence was also reported by Nordstrom [34], who verified that fiber corrosion led to a decrease of its cross section, which has led to a decrease of the load carrying capacity of SFRC elements. The rate of degradation of SFRC due to fiber corrosion is dependent on several parameters, such as: crack width, exposure environmental conditions, and type of fibers [34].

In the case of SFRC, the fibers are dispersed in all the volume of the material. The fibers that are close to the surface have a very small cement matrix cover thickness [3]. Thus, the corrosion can be viewed in two aspects: the fibers corrosion can promote the formation of cracks that can affect the structural performance; the corrosion at surface can conduct to the appearance of rust spots at the surface on the exposed concrete structures, but does not affect its mechanical properties [19,42]. Surface corrosion can be prevented having conjointly  $W/C \leq 0.5$  and a minimum cover of the fibers of 0.2 mm [3].

The generated expansive forces during the corrosion of fibers are insufficient for the detachment of concrete because, due to its reduced diameter, the increase in volume produced by the oxides resulting from corrosive process is not sufficient to split the surrounding concrete [30]. The small volume of the fiber is insufficient to create the bursting stresses that generally occur during the corrosion of larger steel bar diameters, and, therefore, for well compacted concrete the corrosion of fibers is restricted to the surface of the concrete [23].

The electrical resistivity of concrete is being increasingly used to indirectly evaluate concrete characteristics, such as its permeability to the fluids, chloride ion diffusivity, which can be correlated to the degree of concrete resistance to the detrimental effects of severe environments. The concrete electrical resistivity may also provide useful information regarding the risk of steel fibers corrosion in concrete. According to RILEM TC 154-EMC [39], a linear relationship between the intensity of corrosion and the conductivity of a steel rebar embedded into concrete seems to exist. This type of relationship is expected to exist also in a SFRC, but due to the discrete character of fiber reinforcement it is less pronounced. SFRC presents extremely low resistivity due to high electrical conductivity of steel fibers [49]. Concrete resistivity is also affected negatively by the moisture and fiber content [31]. The exposure of fiber reinforced concrete (FRC) to high temperatures increases the risk of reinforcement corrosion [22,29].

### 3. Experimental program

#### 3.1. Materials and mix composition

In the current experimental program, two different concrete mixtures were produced, one of SCC and another one of SFRSCC, using CEM I 42.5 R Portland cement (C), limestone filler (LF), fine river sand (FS) (maximum aggregate size of 1.19 mm and fineness modulus of 1.91), coarse river sand (CS) (maximum aggregate size of 4.76 mm and fineness modulus of 3.84) and crushed granite 5–12 mm (CA) (maximum aggregate size of 19.10 mm and fineness modulus of 6.64), water (W), superplasticizer (SP) based on ether polycarboxylate (ViscoCrete 3005) and hooked ends steel fibers of a length ( $l_f$ ) of 35 mm, a diameter ( $d_f$ ) of 0.50 mm, an aspect ratio ( $l_f/d_f$ ) of 70 and a yield stress of 1300 MPa. Table A1 presents some physical characteristics of the cement and limestone filler.

The method used for defining the composition of the SCC and the SFRSCC, the mixing procedure and other properties of the SCC and the SFRSCC in the fresh state can be found elsewhere [4] and is based on packing density optimization. Table A2 includes the composition that has best fitted self-compacting requirements for SCC without steel fibers and for SFRSCC according with the adopted fiber content ( $C_f$ ). Remark that, in Table A2,  $W/C$  is the water/cement ratio and the value adopted was 0.31, resulted from previous concrete composition studied to obtain a concrete with a good mechanical behavior and durability characteristics, respecting the requirements of workability and resistance to segregation [4].

The specimens of SCC and SFRSCC were molded with dimensions to respect the specifications of the different standards used, which impose specific dimensions for each test. After casting, the filled molds were kept for 3 days in a laboratory envi-

ronment (temperature of 21 °C and relative humidity of 60%), with the exposed face protected with an adherent film, after which they were demolded and stored immersed in water at 20 °C until testing.

#### 3.2. Test procedures

##### 3.2.1. Fresh state

To characterize the concrete behavior in fresh state, slump flow tests were performed according to EN 12350-8 [14], L-Box tests according to EN 12350-10 [11], and tests to achieve density and air content according to EN 12350-6 [12] and EN 12350-7 [13], respectively.

##### 3.2.2. Mechanical properties

The mechanical characterization of the produced mixtures was focused on the study of the variation over time (7, 28 and 90 days) of the elasticity modulus, compressive strength and flexural behavior.

The elasticity modulus and the concrete compressive strength were assessed according to prEN 12390-13 [35] and EN 12390-3 [15], respectively. The tests were carried out using four cylindrical specimens of 150 mm diameter and 300 mm in height, at each age. The bending behavior was assessed, at each age, in four rectangular prisms ( $150 \times 150 \times 600 \text{ mm}^3$ ) according to the recommendations of RILEM TC 162-TDF [40].

##### 3.2.3. Durability properties

Durability test indicators were also assessed by performing durability tests on specimens of SCC and SFRSCC at 28 days of age. These tests were focused on the determination of water absorption by immersion and by capillarity, permeability to air, electrical resistivity, chloride diffusion by migration under non-steady state, resistance to chloride penetration by immersion and carbonation.

The water absorption test by immersion and by capillarity followed the Portuguese Specifications LNEC E394 [26], LNEC E393 [25], respectively, which are based on the RILEM CPC11.2 [38] recommendation. For each composition 3 cubic specimens with 100 mm edge were tested.

The permeability to air was performed using the permeator developed at Leeds University [7]. For these tests 6 cylindrical specimens of 50 mm diameter and 40 mm thickness, extracted from a slab of each composition, were used.

Before the determination of the elasticity modulus and the compressive strength, the electrical resistivity in these specimens was assessed according with the recommendations of RILEM TC 154-EMC [39] specification. The surface electrical resistivity of the SCC and SFRSCC was measured in water-saturated specimens using a four-point Wenner array probe resistivity meter.

To determine the resistance against chloride penetration of these concretes, an accelerated non-steady state migration test method was executed according the Portuguese Specification LNEC E463 [27]. Three cylindrical specimens of 100 mm diameter and 50 mm thickness of each composition were tested. The resistance to chloride penetration by immersion was also assessed by natural diffusion according to the Portuguese Specification LNEC E390 [24]. Two cylindrical specimens of 100 mm diameter and 100 mm thickness of each composition were used. The diffusion coefficient was determined from the non-steady state using Fick's second law.

The determination of the potential carbonation resistance was assessed by an accelerated carbonation method, applied to one rectangular prism ( $100 \times 100 \times 600 \text{ mm}^3$ ) of each composition, following the draft technical specification FprCEN/TS 12390-12 [18].

## 4. Results and discussion

#### 4.1. Fresh state

Regarding the properties in fresh state, the results of slump-flow test and L-Box test are presented in Table A3. Density and air content were also determined and the results are in this table.

As expected, the addition of fibers to fresh SCC resulted in a slight loss of workability, mainly when self-compacting requirements are based on time indicator [14]; however, it was not significant. Both compositions verified the self-compacting requirements and presented almost equal results in terms of spread and  $H_2/H_1$  parameter [11]. For the developed compositions, no visual sign of segregation was detected and the mixtures showed good homogeneity and cohesion. The addition of steel fibers to fresh SCC did not affect the density and the air content of the SCC. This is due to the relatively low percentage of fibers in the composition (2.5% by weight) that does not modify the density, and due to the use of high amounts of fines and the good quality of aggregates in order to

**Table A1**

Physical characteristics of the cement and the limestone filler.

Physical characteristics	Cement	Limestone filler
Specific weight ( $\text{kg/m}^3$ )	3150	2360
Blaine specific surface ( $\text{m}^2/\text{kg}$ )	3873	3879
Fineness (%)	2.00	77.18

**Table A2**  
Compositions for 1 m<sup>3</sup> of concrete.

	C (kg)	LF (kg)	FS (kg)	CS (kg)	CA (kg)	W (L)	SP (L)	C <sub>f</sub> (kg)	W/C
SCC	413	353	198	722	648	127.8	7.83	0	0.31
SFRSCC	413	353	195	713	640	127.8	7.83	60	0.31

**Table A3**  
Fresh properties of SFRSCC and SCC.

Concrete	Slump flow		L-Box			Density (g/cm <sup>3</sup> )	Air content (%)
	Spread (mm)	T <sub>500</sub> (s)	H <sub>2</sub> /H <sub>1</sub>	T <sub>200</sub> (s)	T <sub>400</sub> (s)		
SCC	673	10.2	0.88	2.5	5.3	2.38	0.83
SFRSCC	667	15.6	0.81	5.3	10.1	2.40	0.80

obtain a self-compacting concrete, which allow obtaining low values of air content.

#### 4.2. Hardened state

##### 4.2.1. Mechanical properties

**4.2.1.1. Compressive behavior.** The modulus of elasticity and the compressive strength of each concrete were assessed at 7, 28 and 90 days of age (since casting). In terms of compressive tests, the procedure adopted consisted on determining the compressive strength in one specimen, at each age, in order to establish the maximum load value of the load-unload cycles to be carried out for the determination of the modulus of elasticity. For the three remaining specimens, the modulus of elasticity was determined in a first phase, and then tested up to an axial strain level much higher than the strain at peak stress in order to determine the stress-strain response of the materials not only in the pre-peak but also in the post-peak phase (Fig. B1).

The assessment of the compressive stress-axial strain relationship of SCC and SFRSCC specimens was carried out in a servo-controlled equipment, with a maximum load carrying capacity of 2250 kN. The procedure was executed using the axial displacement as control variable, measured by the internal displacement transducer of the loading equipment.

The average stress-strain curves obtained from a set of four specimens of SCC and SFRSCC are depicted in Fig. B1, while mean values of the elasticity modulus,  $E_{cm}$ , and of the compressive strength,  $f_{cm}$ , at 7, 28 and 90 days of age are included in Table A4. The corresponding coefficients of variation, CoV, are also presented in this table.

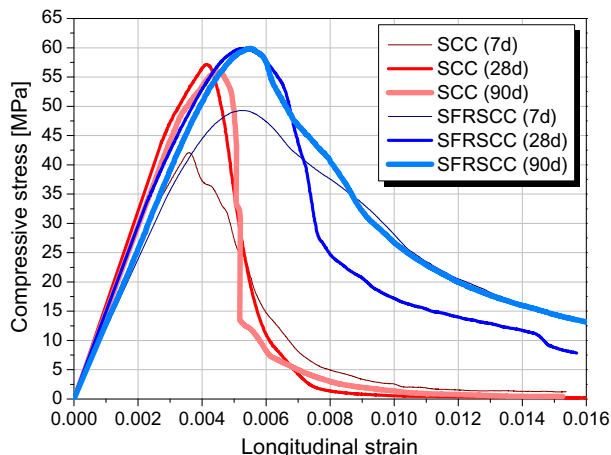


**Fig. B1.** Compressive stress-axial strain relationships at different ages.

**Table A4**  
Relevant results of compression tests.

	SCC			SFRSCC		
	7 days	28 days	90 days	7 days	28 days	90 days
$E_{cm}$ (MPa)	31.16	35.79	36.65	31.58	36.88	37.80
CoV (%)	8.62	1.16	6.96	7.62	6.71	6.38
$f_{cm}$ (MPa)	43.23	60.28	63.85	50.17	61.90	66.13
CoV (%)	8.29	1.27	2.05	6.92	6.34	9.99

As expected, for both compositions the  $E_{cm}$  and the  $f_{cm}$  increased with age, more pronouncedly up to 28 days of age. The addition of steel fibers to SCC caused a slight increase of the elasticity modulus of the concrete due to the small percentage of fibers in SFRSCC composition.

Fig. B1 demonstrates that the addition of steel fibers has mainly contributed towards the increase of the residual compressive strength in the post peak phase of the material, with a favorable effect in terms of its energy absorption capability.

To estimate the elasticity modulus and the compressive strength of plain concrete (PC) at various ages,  $E_{cm}(t)$  and  $f_{cm}(t)$ , respectively, the Eurocode 2 [17] suggests the followings equations:

$$E_{cm}(t) = (f_{cm}(t)/f_{cm}(28))^{0.3} \times E_{cm}(28) \quad (1)$$

$$f_{cm}(t) = f_{cm}(28) \times \exp \left\{ 0.20 \left[ 1 - \left( \frac{28}{t} \right)^{1/2} \right] \right\} \quad (2)$$

where  $E_{cm}(28)$  and  $f_{cm}(28)$  are the average elasticity modulus and compressive strength at 28 days.

Figs. B2 and B3 present the predicted evolution of the elasticity modulus and the compressive strength of SCC and SFRSCC, respectively, according to EC2. In order to use the Eqs. (1) and (2), the values obtained experimentally for  $E_{cm}(28)$  and  $f_{cm}(28)$  in SCC and SFRSCC were considered. Figs. B2 and B3 demonstrate that no significant differences between the elasticity modulus and the compressive strength of SCC and SFRSCC, obtained experimentally and provided to Eurocode 2, were detected, except in the early ages, due to the high volume of ultra-thin material, such as calcareous filler, included in these compositions. Cunha *et al.* [10] have adjusted the equations proposed by Eurocode 2 in order to be capable of simulating the time evolution of the Young's modulus and compressive strength of SCCs.

**4.2.1.2. Flexural behavior.** The flexural behavior of SFRSCC was characterized according to the recommendations of RILEM TC 162-TDF [40] and CEB FIP Model Code [8]. The bending tests were performed following the proposal of RILEM TC 162-TDF [40] in

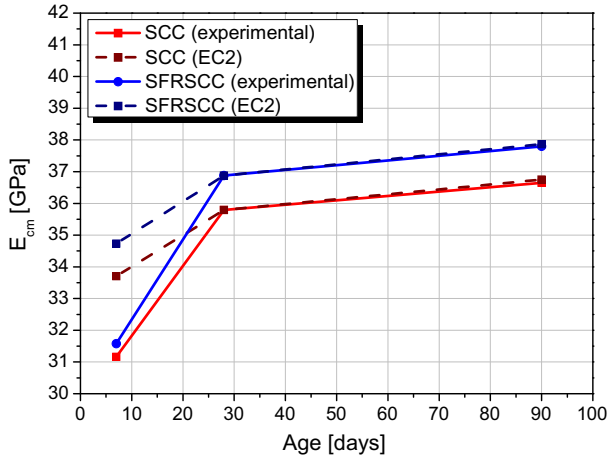


Fig. B2. Variation of the elasticity modulus of the SCC and SFRSCC with the age, obtained experimentally and according to the Eurocode 2.

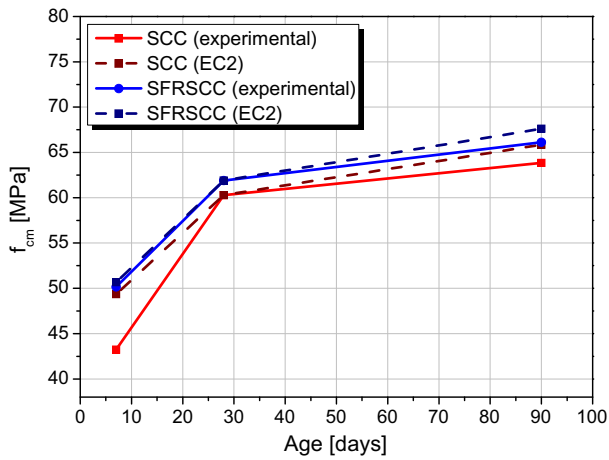


Fig. B3. Variation of the compressive strength of the SCC and SFRSCC with the age, obtained experimentally and according to the Eurocode 2.

terms of curing procedures, position and dimensions of the notch sawn into the specimen, load and specimen support conditions, characteristics for both the equipment and measuring devices, and test procedures. The three-point bending tests were performed in displacement control by imposing a deflection rate of 0.2 mm/min in the transducer positioned at midspan of the beam (Fig. B4). A line load was applied along the width of the beam at



Fig. B4. Test setup of the bending test.

the midspan (loading length of 150 mm). Four beams of each composition, with  $150 \times 150 \text{ mm}^2$  cross section and a length of 600 mm were used. The notch at midspan was produced on one of the faces perpendicular to the casting surface. The width of the notch was 5 mm, and the depth 25 mm, leaving a section with a depth of 125 mm at midspan. The distance between the two roller supports was 500 mm.

Fig. B5 represents the average force–deflection response ( $F - \delta$ ) registered in the SCC and SFRSCC at the three considered ages. Analyzing the curves obtained in SCC beams, it is verified that just after the peak load, an abrupt load decay has occurred in all the SCC specimens, due to the brittle character of this material. However, in SFRSCC beams the increase in ductility provided by the incorporation of fibers is clear. The fibers were very effective in terms of increasing the flexural strength, the post peak resistance, and the energy absorption.

From the obtained force–deflection relationship, the proportionality limit ( $f_{ct,L}$ ), the equivalent ( $f_{eq,2}$  and  $f_{eq,3}$ ) and the residual ( $f_{R,1}$  and  $f_{R,4}$ ) flexural tensile strength parameters were calculated. According to RILEM TC 162-TDF [40], the parameters  $f_{eq,2}$  and  $f_{eq,3}$  are related to the material energy absorption capacity up to a deflection of  $\delta_2$  and  $\delta_3$  ( $\delta_2 = \delta_L + 0.65 \text{ mm}$  and  $\delta_3 = \delta_L + 2.65 \text{ mm}$ , where  $\delta_L$  is the deflection corresponding to the highest load,  $F_L$  recorded up to a deflection of 0.05 mm) provided by fiber reinforcement mechanisms ( $D_{BZ,2}^f$  and  $D_{BZ,3}^f$ ), as seen in Fig. B6. The parcel of the energy due to matrix cracking ( $D_{BZ}^c$ ) is not considered in the  $f_{eq}$  evaluation (Vandewalle et al. [52]). The parameters  $f_{R,1}$  and  $f_{R,4}$  are the stresses for the forces  $F_{R,1}$  and  $F_{R,4}$ , respectively, at deflections of  $\delta_{R,1} = 0.46 \text{ mm}$  and  $\delta_{R,4} = 3.0 \text{ mm}$ , according to RILEM TC 162-TDF, and at CMOD (crack mouth opening displacement) of  $\text{CMOD}_1 = 0.5 \text{ mm}$  and  $\text{CMOD}_4 = 3.5 \text{ mm}$  according to CEB FIP Model Code [8].

According to RILEM TC 162-TDF [40] and CEB-FIP Model Code [8], the limit of proportionality, the equivalent and the residual flexural tensile strength parameters are obtained from the following equations:

$$f_{ct,L} = \frac{3F_L L}{2bh_{sp}^2} \quad (3)$$

$$f_{eq,2} = \frac{3}{2} \left( \frac{D_{BZ,2}^f}{0.50} \right) \frac{L}{bh_{sp}^2}; \quad f_{eq,3} = \frac{3}{2} \left( \frac{D_{BZ,3}^f}{2.50} \right) \frac{L}{bh_{sp}^2} \quad (4)$$

$$f_{R,1} = \frac{3F_{R,1} L}{2bh_{sp}^2}; \quad f_{R,4} = \frac{3F_{R,4} L}{2bh_{sp}^2} \quad (5)$$

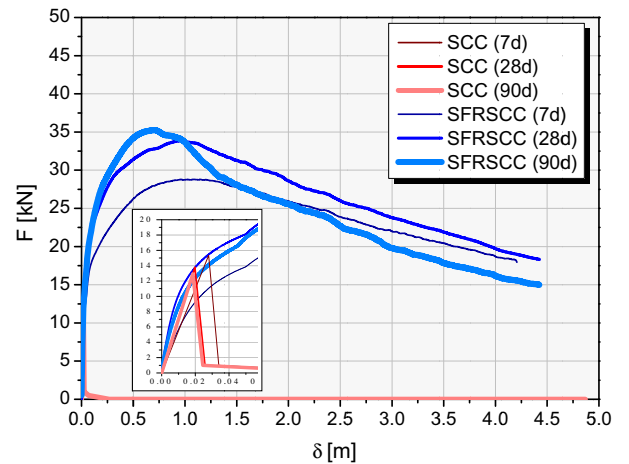


Fig. B5. Flexural load–deflection relationships at different ages.

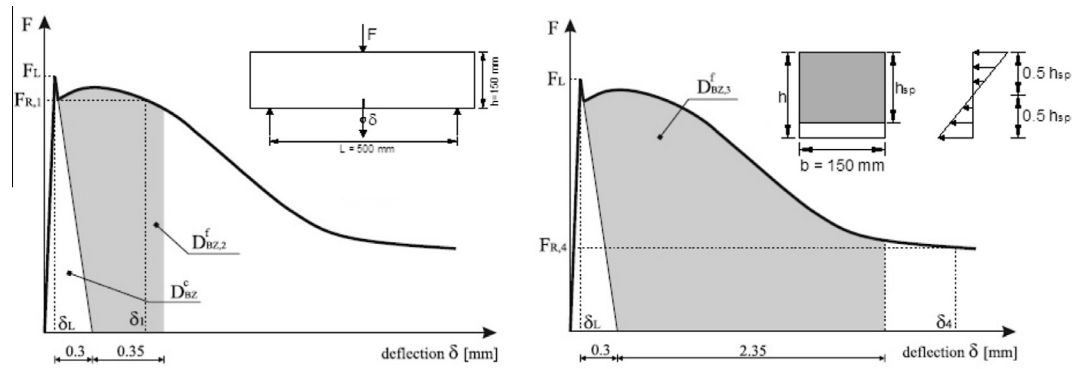


Fig. B6. Load-deflection diagrams for the determination of the equivalent and residual flexural tensile strength parameters [33].

The results obtained are presented in Table A5 and show that both  $f_{eq}$  and  $f_R$  have increased up to 28 days, and for 90 days a decrease was registered, mainly for the parameters evaluated at larger deflection/crack width, which means that due to the relatively high strength of the matrix some fibers would have failed by rupture. Comparing the results of the residual resistance,  $f_R$ , calculated according to RILEM and the CEB-FIP, the difference is insignificant.

#### 4.2.2. Durability indicators

4.2.2.1. *Water absorption by immersion.* The water absorption by immersion was determined according to the Portuguese Standard LNEC E394 [26]. The test consisted in two major steps: saturating the specimens after drying. First, the specimens were dried in a ventilated oven at a temperature of  $105 \pm 5$  °C until the difference in mass during 24 h was less than 0.1%. The dry mass was called  $M_d$ . Afterwards, the specimens were immersed in water until the change in mass during 24 h was less than 0.1%. The obtained saturated mass was called  $M_s$ . The water absorption by immersion ( $W_i$ ) was calculated from the following equation:

$$W_i = \frac{(M_s - M_d)}{(M_d - M_h)} \quad (6)$$

where  $M_h$  is the hydrostatic mass of the specimen immersed in water.

Fig. B7 presents the test results of water absorption by immersion, which indicates that the open porosity of SFRSCC was slightly higher than of SCC (5.6%). The average porosity of the SCC and SFRSCC was 10.7% and 11.3%, respectively. This allows concluding that the addition of fibers to SCC did not cause a significant increase of the open porosity, due to the homogeneous microstructure of these concretes, in the context of water absorption.

4.2.2.2. *Water absorption by capillarity.* The water absorption by capillarity was determined according to the Portuguese Standard LNEC E393 [25]. The test consisted in measuring during three days

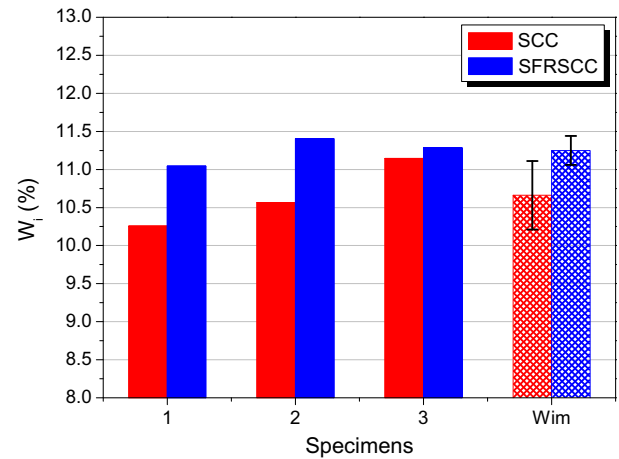


Fig. B7. Water absorption by immersion at atmospheric pressure.

the velocity of water absorption in no saturated concrete and immersed in a height of  $5 \pm 1$  mm of water. The water absorbed by capillarity,  $W_c$ , was determined by the ratio between the increase of the mass specimen by the area of the lower surface of the specimen,  $\Omega_i$  that was in contact with the water, according the following equation:

$$W_c = \frac{(M_i - M_0)}{\Omega_i} \quad (7)$$

where  $M_i$  is the mass of the specimen in contact with water for different times of reading ( $\sqrt{t_i}$ ) and  $M_0$  is the dry mass of the specimen at  $40 \pm 5$  °C.

The results in terms of amount of water absorbed per unit area versus square root of time are presented in Fig. B8. The coefficient of water absorption by capillarity action, which corresponds to the slope of these curves during the initial 4 hours of testing, is

Table A5  
Relevant results of flexural tests.

	$f_{ct,L}$ (MPa)	$f_{eq,2}$ (MPa)	$f_{eq,3}$ (MPa)	RILEM TC 162 TDF		CEB-FIP Model Code	
				$f_{R,1}$ (MPa)	$f_{R,4}$ (MPa)	$f_{R,1}$ (MPa)	$f_{R,4}$ (MPa)
AVG (7d)	5.09	8.34	8.51	8.25	7.09	8.39	6.56
CoV (%)	5.27	20.28	19.41	19.00	27.29	18.26	30.14
AVG (28d)	6.39	10.12	9.72	9.92	7.63	10.05	7.05
CoV (%)	7.58	19.73	15.25	19.37	13.03	18.72	11.86
AVG (90d)	7.01	10.11	7.94	9.82	7.55	9.99	6.90
CoV (%)	5.75	4.50	12.85	3.62	4.97	18.78	20.35

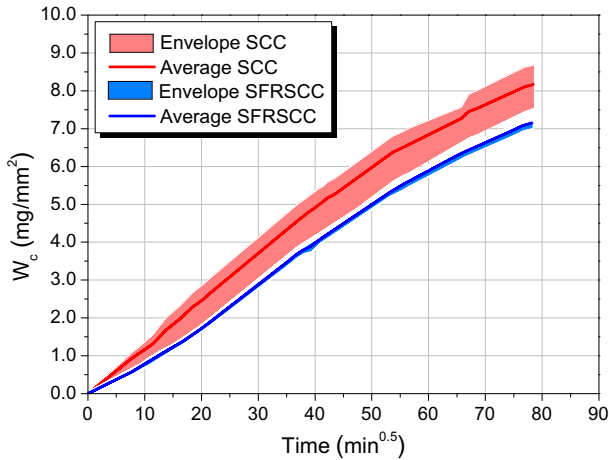


Fig. B8. Water absorption by capillarity of SCC and SFRSCC.

0.1272 mg/mm<sup>2</sup>/min<sup>0.5</sup> for SCC and 0.0941 mg/mm<sup>2</sup>/min<sup>0.5</sup> for SFRSCC. As represented in Fig. B8, the total amount of water absorbed is greater in SCC than in SFRSCC, but the coefficient of water absorption by capillarity,  $K_C$  is similar in both compositions, which mean that the presence of fibers did not cause a substantial change in the capillary porosity of SFRSCC surface, in order to facilitate the penetration of deteriorating agents.

4.2.2.3. *Air permeability.* For the determination of air permeability, the Leeds cell was used. This device ensures that the specimen is subjected to a steady state flow of the fluid that passes through the sample under a given pressure during a certain period of time (Fig. B9). For gases, the coefficient of permeability,  $K_G$  is determined based on the modified D'Arcy law, according with the following equation, which considered the compressibility and the viscosity of the fluid.

$$K_G = \frac{2v \times \eta \times L \times P_2}{A(P_1^2 - P_2^2)} \quad (8)$$

where  $v$  is gas flow,  $\eta$  is the dynamic viscosity of the gas (considered  $2.02 \times 10^{-16}$  Ns/m<sup>2</sup>),  $L$  is the thickness of the concrete cross section crossed by the gas,  $A$  is the cross section of concrete crossed by the gas,  $P_1$  is the absolute pressure gas inlet (adopted 3 bar) and  $P_2$  is the absolute pressure gas outlet (atmospheric pressure – 1 bar).

Fig. B10 presents the air permeability coefficients of the tested specimens. The average of air permeability coefficient was  $0.483 \times 10^{-16}$  m<sup>2</sup> for SCC and  $0.443 \times 10^{-16}$  m<sup>2</sup> for SFRSCC. These results are similar because the variation of 8.3% between them is

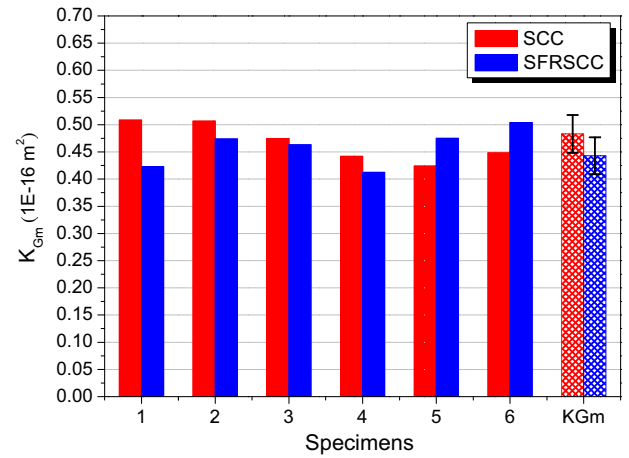


Fig. B10. Air permeability coefficients for the specimens.

of the order of magnitude of the test error, since this type of test has usually high dispersion of results. This allows concluding that the addition of fibers to SCC does not seem to influence the air permeability of this type of concrete, provided that the composition is properly optimized, as in it was the case in the present work.

4.2.2.4. *Electrical resistivity.* The surface electrical resistivity of SCC and SFRSCC was measured in water-saturated specimens using a four-point Wenner array probe resistivity meter. In this device two end electrodes are used to inject current, and the voltage is measured between the two inner electrodes (Fig. B11). The electrical resistivity,  $\rho$ , is calculated according to the following equation:

$$\rho = 2 \times \pi \times a \times \frac{V}{I} \quad (9)$$

where  $a$  is the distance between the two inner electrodes,  $V$  is the potential difference measured, and  $I$  is the applied current.

The average electrical resistivity,  $\rho_m$ , of the tested concretes is presented in Table A6. The difference between SCC and SFRSCC (reduction of 63% in SFRSCC) was obtained due to the high electrical conductivity of steel fibers, which decreases the electrical resistivity of concrete. The values of electrical resistivity have increased with the age of the concrete in both compositions, and at 90 days the process seems not yet stabilized. The high CoV obtained in SFRSCC at 7 and 28 days is clarified by the presence of steel fibers that can significantly influence the electrical field generated by Wenner resistivity meter.

The interpretation of the electrical resistivity indicated in RILEM TC 154-EMC [39] specification seems not valid for SFRSCC, since

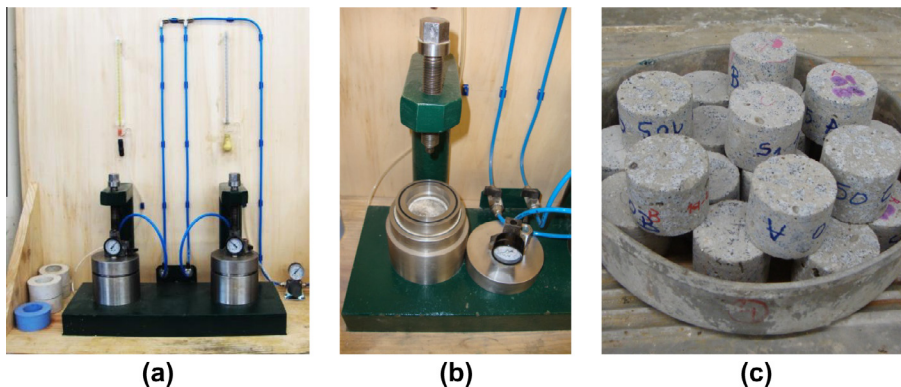


Fig. B9. Leeds cell (a and b) and specimens used (c).

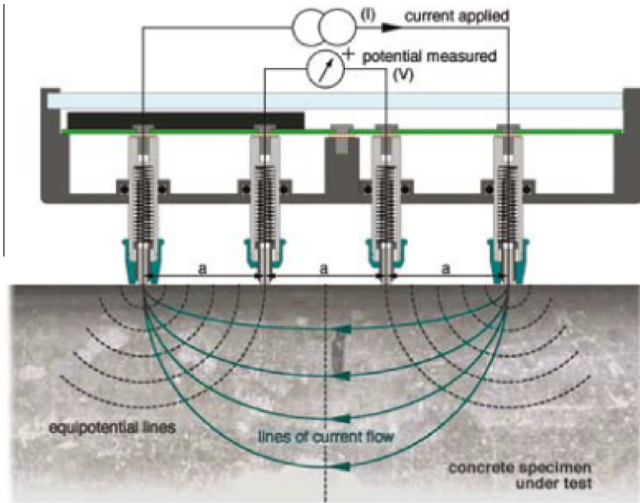


Fig. B11. Testing of electrical resistivity with Wenner resistivity meter.

Table A7  
Results of chloride migration test.

	SCC	SFRSCC
$D_m (\times 10^{-12} \text{ m}^2/\text{s})$	10.27	11.61
CoV (%)	1.49	30.93

$$D_m = \frac{0.0239(273 + T) \times L}{(U - 2) \times t} \left( x_d - 0.0238 \sqrt{\frac{(273 + T) \times L \times x_d}{U - 2}} \right) \quad (10)$$

where  $T$  is the mean value between initial and final temperature of the anolyte solution,  $U$  is the absolute value of the potential difference,  $L$  is the thickness of specimen,  $t$  is test duration and  $x_d$  is the average penetration depth.

The average diffusion coefficient of chlorides by migration,  $D_m$ , is shown in Table A7, indicating that the resistance to penetration of chlorides is apparently the same in SCC and in SFRSCC, but the relatively high COV for the SFRSCC does not allow extracting conclusive conclusions in this respect. In any case, the accumulation of chloride ions in the fiber-paste interface deteriorates the protective oxide film of the steel fibers, leaving them more vulnerable to corrosion. During the test it was possible to observe the formation of corroded material in the cathode solution of the tests of SFRSCC and it was increased with the duration of the test (Fig. B12b).

4.2.2.6. Corrosion of steel fibers. With the purpose of verifying if the corrosion of fibers may or may not lead to cracking and subsequent spalling of the surrounding concrete, SFRSCC specimens were submitted to the migration test of chlorides, as presented in the previous section, in order to induce severe corrosion in steel fibers. For this purpose, some samples were subjected to a potential difference of 30 V for 72 h, and others at 45 V for 72 h. With the migration of these chlorides under extremely aggressive conditions, it was detected that the cathodic solution showed increasing signs of corrosion of steel fibers (Fig. B13a and b). After 72 h of testing, the SFRSCC specimens showed strong evidence of corrosion on the surface, as intense as the most aggressive environment (Fig. B14a). The cross section of the steel fibers seems to have decreased along the chloride penetration length in the specimen (Fig. B14b). It was also noted that after migration test, SFRSCC specimens presented micro-cracks along the outer surface (Fig. B15a). This might have been caused by the increase in fiber volume associated with the corrosion of the fibers since, as known, the formation of iron oxide involves an increase in fiber volume.

After the exposure period, the splitting tensile strength was determined according to EN 12390-6 [16]. At the section fracture of the specimens it was observed an intense corrosion of steel fibers and the dominant failure mode was fiber rupture (Fig. B15b).

Table A6  
Results of the electrical resistivity tests.

	SCC			SFRSCC		
	7 days	28 days	90 days	7 days	28 days	90 days
$\rho_m$ (k cm)	7.3	10.1	11.4	2.6	3.7	4.5
CoV (%)	2.71	1.64	3.46	22.75	21.47	4.01

the type and amount of steel fibers should be considered whose high conductivity influences the resistivity measurement.

4.2.2.5. Diffusion of chlorides by migration under non-steady state. To test the resistance against chloride penetration, an accelerated non-steady state migration test method was applied according to the Portuguese Standard LNEC E463 [27]. The principle of this test is to apply, axially, an external electrical potential across the specimen, by forcing the chloride ions outside to migrate into the specimen (Fig. B12a and b). After 24 h test duration, the specimen is axially split and a silver nitrate solution is splayed on to one of the freshly split sections (Fig. B12c). The chloride penetration depth can then be measured from the visible white silver chloride precipitation, after which the chloride migration coefficient can be calculated from this penetration depth. The catholyte solution is 10% NaCl (2 N) by mass in tap water and the anolyte solution is 0.3 N NaOH in tap water. The determination of the chloride migration coefficient  $D_m$  is given by the following equation:

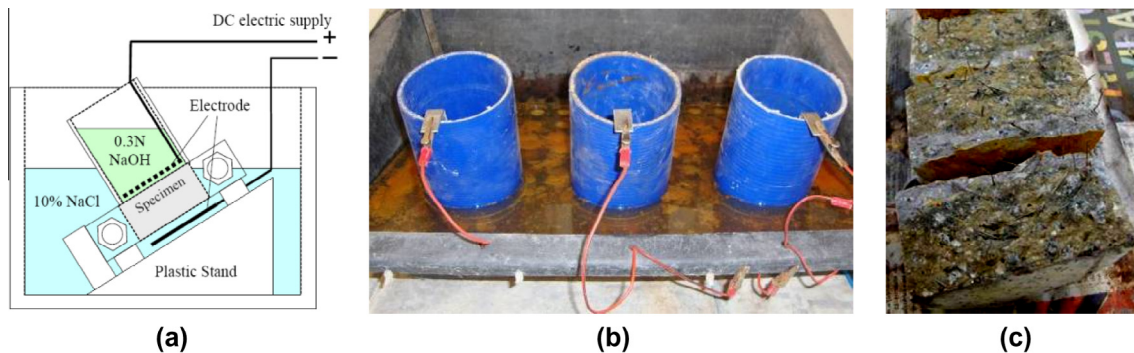


Fig. B12. Rapid chloride migration test.

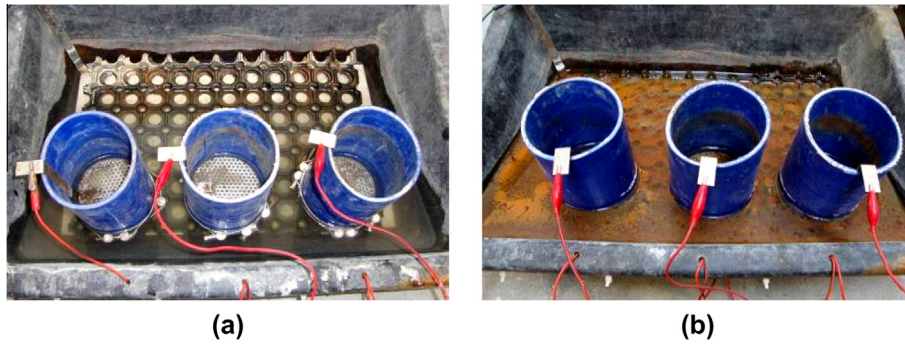


Fig. B13. Chloride migration test of SFRSCC at the beginning (a) and at the end (b).



Fig. B14. SFRSCC specimens after and before chloride migration test (a) and after tensile test by diametral compression (b).



Fig. B15. Micro-cracking observed in SFRSCC specimens after chloride migration test (a) and fracture surface after diametral compression test (b).

The splitting tensile strength,  $f_{ct}$ , by diametral compression tests are presented in Table A8. The results shown in Table A8 indicate that the tensile strength by diametral compression of SFRSCC was not significantly affected by steel fibers corrosion when these fibers were partially corroded (30 V). When the fibers were fully corroded (45 V), the corrosion of the fibers caused intense damage in the surrounding medium by the formation of micro-cracks, with a consequent reduction in tensile strength by diametral compression of SFRSCC (44%) compared to concrete without corroded fibers. Since fiber rupture was the dominant failure mode in the SFRSCC specimens subjected to 45 V, the reduction of the cross sectional area of fibers due to corrosion seems to have had a more intense effect than the fiber bond degradation due to micro-spalling formed around the corroded fibers.

The tests conducted in extreme aggressiveness conditions allowed to evidence that corrosion of steel fibers may induce the formation of micro-cracks in surrounding concrete and subsequent micro-spalling, with a detrimental effect in terms of matrix resistance.

Table A8

Splitting tensile strength from diametral compression tests.

	SFRSCC (without corrosion)	SFRSCC (30 V – 72 h)	SFRSCC (45 V – 72 h)
$f_{ct}$ (MPa)	5.59	5.67	3.13
CoV (%)	16.71	15.81	9.12

Evaluating the weight of the specimens before and after the test, an increase in mass was observed of 0.80% in the first case (30 V) and 1.51% in the second case (45 V). However, it should be noted that this damage was obtained for extreme aggressiveness conditions, which are not expected to occur in real environmental conditions.

4.2.2.7. Resistance to chloride penetration by immersion. The determination of the resistance to chloride penetration by natural immersion was performed according to the Portuguese Standard

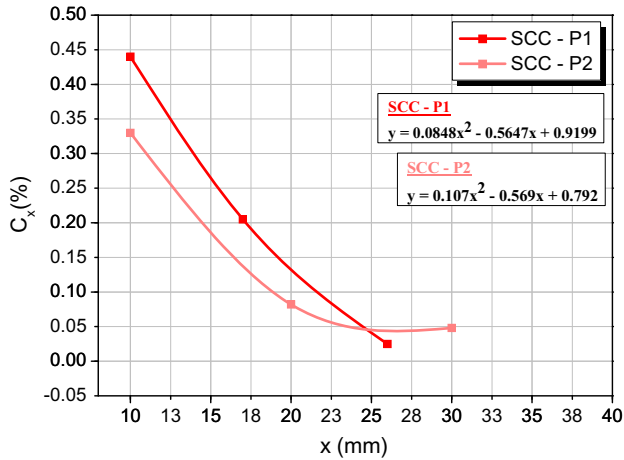


Fig. B16. Chloride profile in SCC.

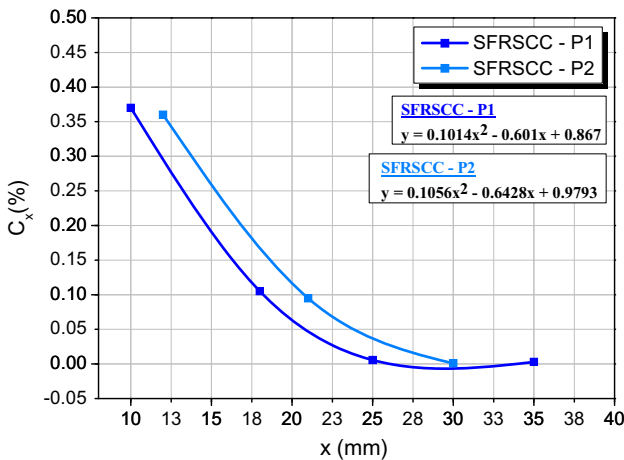


Fig. B17. Chloride profile in SFRSCC.

Table A9  
Results of chloride diffusion test.

	SCC	SFRSCC
$D_d (\times 10^{-12} \text{ m}^2/\text{s})$	11.62	8.21
CoV (%)	3.88	1.66

LNCE E390 [24]. This method is based on determining parameters related to chlorides penetration in hardened concrete, based on measuring the chloride penetration profile in samples after immersion in a calcium hydroxide saturated solution containing 15% of

sodium chloride. The determination of the chloride concentration at different depths was performed using the kit RCT-500 (Rapid Chloride Test) by using the German Instruments A/S. This test took relatively long time (90 days of immersion).

The test gives the values of diffusion coefficient,  $D_d$ , and the surface chloride content,  $C_s$ , by curve-fitting the measured chloride profile to an error-function solution of Fick's 2<sup>nd</sup> law, according to the following equation:

$$C_x = C_s - (C_s - C_0) \operatorname{erf} \left( \frac{1/2x}{\sqrt{D_d t}} \right) \quad (11)$$

where  $C_x$  is the chloride content measured at depth  $x$  for a time of immersion  $t$ ,  $C_s$  is the chloride content calculated at the concrete surface after a time of immersion  $t$ ,  $C_0$  is the initial chloride content in concrete and  $\operatorname{erf}$  is the error-function.

The chloride profile obtained in SCC and in SFRSCC is presented in Figs. B16 and B17, respectively, and the average diffusion coefficient of chlorides by natural diffusion,  $D_d$ , is included in Table A9. The values present evidence that the resistance to penetration of chlorides is higher in SCC than in SFRSCC, since the presence of the steel fibers caused the setting of chloride ions on the fibers, delaying or even preventing the penetration of ions into the matrix. Comparing the values of  $D_d$  with the values of  $D_m$  presented in the Table A7, the trend is exactly opposite. However, the method of evaluation by migration, despite being faster than the one based on diffusion by natural immersion, has some disadvantages, since the results are qualitative (the potential difference applied and the duration of test are defined according with some preliminary measures of current intensity obtained in plain concrete) and cause an increase of temperature in concrete. Thus, it is more prudent to use methods based on the diffusion immersion to evaluate the penetration of chlorides in SFRSCC, which although it takes longer testing periods, it represents the best environment for current exposures.

4.2.2.8. Carbonation. The evaluation of the potential carbonation resistance in SCC and SFRSCC beams was carried out using an accelerated carbonation test. After a period of preconditioning, the test was carried out under controlled exposure conditions on specimens placed in a storage chamber with 5,0 (±0,5)% of carbon dioxide, 20 (±2) °C temperature, and 55 (±5)% relative humidity for a period of 294 days (Fig. B18a). The measurement of the carbonation depth was performed according to the European Standard FprCEN/TS 12390-12 [18], using the phenolphthalein solution by spraying the indicator on the split surface of the beam at different ages of exposure (Fig. B18b). The solution became a pink color in the uncarbonated concrete, providing a differentiation from the carbonated concrete, giving a distinct boundary marking the carbonation front (Fig. B18c).

Figs. B19 and B20 show the average carbonation depths (mm<sup>2</sup>) measured on SCC and SFRSCC until the exposure period of 294 days

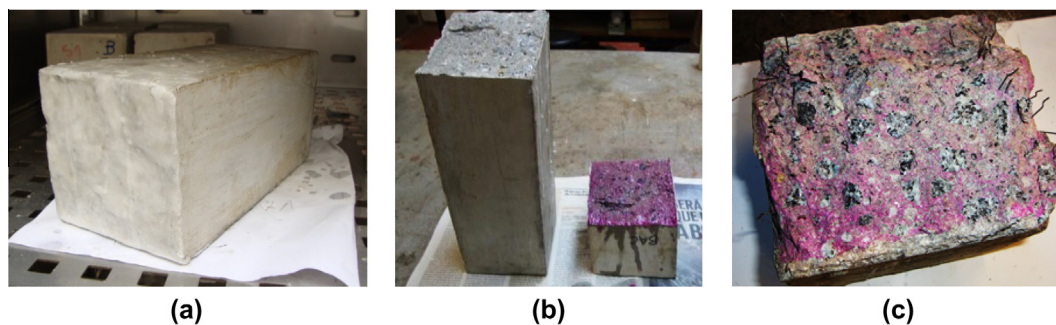


Fig. B18. Procedure for obtaining the carbonation depth.

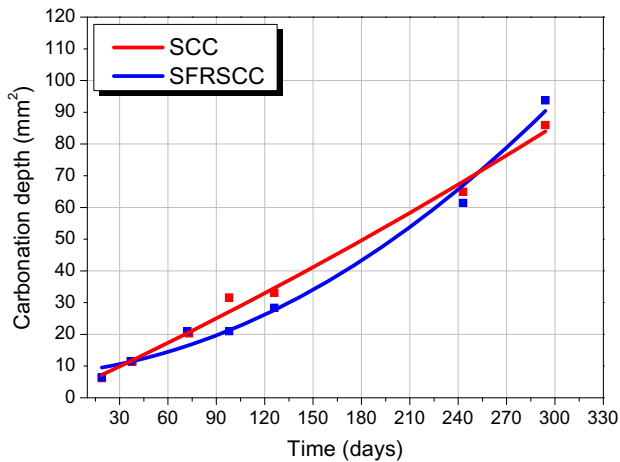


Fig. B19. Carbonation depth along exposed time (294 days).

and 70 days, respectively. In Fig. B19, it is possible to see that the carbonation depth does not have a completely linear time-evolution over the maximum period of exposure adopted (294 days). However, until 70 days of exposure (period indicated by the specification), there was linear time-evolution penetration of  $\text{CO}_2$ , as seen in Fig. B20.

The carbonation resistance,  $R_{c65}$ , was calculated by the following equation, according with the recommendations of the Portuguese Standard LNEC E465 [28]:

$$R_{c65} = \frac{2 \times C_{\text{accel}} \times t_1}{X_1^2} \quad (12)$$

where  $C_{\text{accel}}$  is the  $\text{CO}_2$  concentration to accelerate the carbonation process ( $90 \times 10^{-3} \text{ kg/m}^3$ ),  $t_1$  is the necessary time to reach a value of carbonation depth  $X_1$  in the specimen (adopted 70 days).

The obtained carbonation resistance of SCC ( $1774.62 \text{ kg year/m}^5$ ) is only 4.66% higher than of SFRSCC ( $1695.67 \text{ kg year/m}^5$ ), which means that they have a similar resistance to carbonation in uncracked stage.

For SCC and SFRSCC there is a low increase of depth of carbonation over time of exposure to  $\text{CO}_2$  due to the reduced permeability of the concrete. In the SCC mixes, the near-surface concrete is denser and more resistant than in the traditional vibrated concrete, which caused this higher resistance to carbonation.

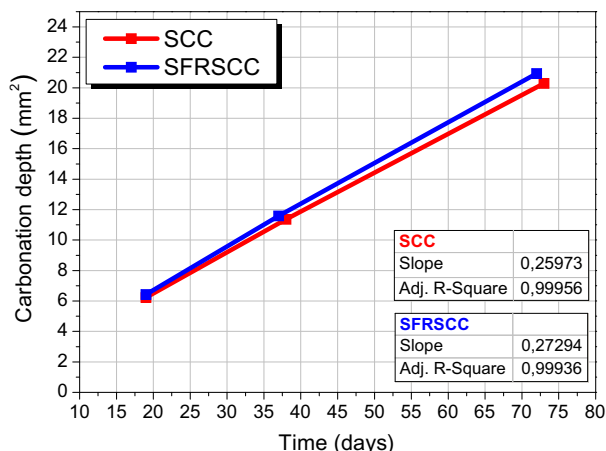


Fig. B20. Carbonation depth along exposed time (70 days).

## 5. Conclusions

Based on the results obtained from mechanical properties and durability indicators, the following observations can be pointed out:

- The addition of steel fibers to fresh SCC in a content of  $60 \text{ kg/m}^3$  did not affect significantly the self-compacting requisites.
- In terms of compressive behavior, the addition of steel fibers to SCC has mainly contributed for the increase of the post peak resistance, with a favorable effect in terms of energy absorption capability of this material.
- The evolution of the elasticity modulus and the compressive strength in SCC and SFRSCC, after 28 days of age, can be estimated according to Eurocode 2.
- The fibers were very effective in terms of increasing the post-cracking flexural resistance and the energy absorption. The values of residual flexural tensile strength,  $f_R$ , calculated according to RILEM were similar to the same values obtained by CEB-FIP.
- The addition of steel fibers resulted in a very slightly increase of open porosity of SCC.
- Adding steel fibers did not change significantly the water absorption by capillarity of SCC, indicating that the capillarity pore size was not substantially changed.
- The air penetrability was not substantially affected by the presence of steel fibers, although a slight reduction in SFRSCC was observed.
- The presence of steel fibers has reduced the electrical resistivity of concrete in 63%.
- Determining the diffusion coefficient from the chloride migration test under non-steady state may not be feasible for a SFRSCC, since the test methodology can cause significant corrosion of steel fibers and chlorides may tend to settle in steel fibers. The determination of the diffusion coefficient for a SFRSCC is more feasible by natural immersion test in salt solution. However, the results obtained in both concretes were similar.
- In conditions of extreme aggressiveness, corrosion of steel fibers can induce cracking in concrete, leading to a decrease of tensile strength for the SFRSCC. However, it should be noted that this damage was obtained in conditions of extreme aggressiveness, which is not expected to occur in real environmental conditions.
- Due to the relatively high compactness of SCC mixes, they presented good resistance to carbonation.

## Acknowledgements

The study reported in this paper is part of the research project QREN number 5387, LEGOUSE – *Development of cost competitive pre-fabricated modular buildings*, involving the Companies Mota-Engil, CiviTest, the ISE/University of Minho and PIEP. The authors wish to acknowledge the support provided by Maccaferri and Radmix for the supplying of the fibers, Sika for the superplasticizer, Secil for the cement and Omya Comital for the limestone filler. The first author acknowledges the research grant under this project.

## Appendix A

See Tables A1–A9.

## Appendix B

See Figs. B1–B20.

## References

- [1] ACI 544.5R-10, Report on the Physical Properties and Durability of Fiber Reinforced Concrete, ACI Committee 544.
- [2] Aldea C, Shah S. Durability enhancements of cracked concrete by fibers. *ACI Spec Publ* 2011;276:1–14.
- [3] Balouch S, Forth J, Granju J. Surface corrosion of steel fibre reinforced concrete. *Cem Concr Res* 2010;17:410–4.
- [4] Barros J, Pereira E, Santos S. Lightweight panels of steel fibre reinforced self-compacting concrete. *J Mater Civ Eng ASCE* 2007;19(4):295–304.
- [5] Berrocal C, Lundgren K, LÖfgren I. Influence of steel fibres on corrosion of reinforcement in concrete in chloride environments: A review, Proceedings of International Conference. FC2013-Fiber Concrete 2013, 12<sup>th</sup>–13<sup>th</sup> September, Prague, Czech Republic.
- [6] Bischoff P. Tension stiffening and cracking of steel fiber-reinforced concrete. *J Mater Civ Eng* 2003;15(2):174–82.
- [7] Cabrera JG. Design and production of high performance concrete, Proceedings of International Conference. Infrastructure Regeneration and Rehabilitation Improving the Quality of Life Through Better Construction, Sheffield; 1999. p. 1–14.
- [8] CEB FIP Model Code 2011, V. 1. p. 350.
- [9] Corinaldesi V, Moriconi G. Durable fiber reinforced self-compacting concrete. *Cem Concr Res* 2004;34:249–54.
- [10] Cunha V, Barros J, Sena-Cruz J. Modelling the influence of age of steel fibre reinforced self-compacting concrete on its compressive behaviour. *RILEM Mater Struct J* 2008;41:465–78.
- [11] EN 12350-10, Testing fresh concrete – Part 10: self-compacting concrete – L-Box test; 2010.
- [12] EN 12350-6, Testing fresh concrete – Part 6: Density; 2009.
- [13] EN 12350-7, Testing fresh concrete – Part 7: determination of air content – Pressuremeter methods; 2009.
- [14] EN 12350-8, Testing fresh concrete – Part 8: Self-compacting concrete – Slump-flow test; 2010.
- [15] EN 12390-3, Testing hardened concrete – Part 3: compressive strength of specimens; 2009.
- [16] EN 12390-6, Testing hardened concrete – Part 6: tensile strength by compression of specimens; 2003.
- [17] EN 1992-1-1, Eurocode 2: design of concrete structures – Part 1-1: General rules and rules for buildings, European Standard, CEN; 2004.
- [18] FprCEN/TS 12390-12, Testing hardened concrete – Part 12: Determination of the potential carbonation resistance of concrete: accelerated carbonation method, Technical Specification, European Committee for standardization, Brussels; 2010.
- [19] Graeff A, Pilakoutas K, Lynsdale C, Neocleous K. Corrosion Durability of Recycled Steel Fibre Reinforced Concrete, Article No.7, Intersections/Intersec\_ii, V. 6, No.4; 2009.
- [20] Granju J, Balouch S. Corrosion of steel fibre reinforced concrete from the cracks. *Cem Concr Res* 2005;35:573–7.
- [21] Hoseini M, Bindiganavile V, Banthia N. The effect of mechanical stress on permeability of concrete: a review. *Cement Concr Compos* 2009;31:213–20.
- [22] Khalil W. Influence of high temperature on steel fiber reinforced concrete. *J Eng Develop* 2006;10(2).
- [23] Lambrechts A, Nemegeer D, Vanbrabant J, Stang H. Durability of steel fibre reinforced concrete, Proceedings of 6<sup>th</sup> CANMET/ACI durability of concrete conference SP212, ACI, Michigan, USA; 2003.
- [24] LNEC E390, Concrete. Determination of resistance to chloride penetration – immersion test, Lisbon: LNEC; 1993. p. 2.
- [25] LNEC E393, Concrete. Determination of water absorption by capillarity, Lisbon: LNEC; 1993. p. 2.
- [26] LNEC E394, Concrete. Determination of water absorption by immersion – test at atmospheric pressure, Lisbon: LNEC; 1993. p. 2.
- [27] LNEC E463, Determination of diffusion coefficient of chlorides by migration under non-steady state, Lisbon: LNEC; 2004. p. 8.
- [28] LNEC E465, Method for estimating the properties of the concrete performance capable of meeting the design life of reinforced concrete structures or prestressed under environmental expositions XC and XS, Lisbon: LNEC; 2007.
- [29] Lourenço L. Fiber Reinforced Concrete: applications and inspection techniques and reinforcement of structural elements affected by the action of a fire, PhD Thesis, University of Minho, Guimarães, Portugal (in Portuguese); 2012.
- [30] Mangat P, Gurusamy K. Chloride diffusion in steel fiber-reinforced marine concrete. *Cem Concr Res* 1987;17:385–96.
- [31] Michel A, Geiker M, Stang H, Olesen J, Solgaard A. Numerical modelling of reinforcement corrosion, influence of steel fibres and moisture content on resistivity and corrosion current density, Proceedings of 3<sup>th</sup> International RILEM PhD Student Workshop on Modelling the Durability of Reinforced Concrete, 22<sup>nd</sup>–24<sup>th</sup> October 2009, Guimarães, Portugal.
- [32] Mindess S, Young JF, Darwin D. *Concrete*. New Jersey: Prentice-Hall; 2002.
- [33] Nemegeer D, Vanbrabant J, Stang H. Brite Euram program on steel fibre concrete subtask: durability: corrosion resistance of cracked fibre reinforced concrete. In: International RILEM Workshop on Test and Design Methods for Steel Fibre Reinforced Concrete; 2003. p. 47–66.
- [34] Nordstrom E. Durability of Sprayed Concrete – Steel fibre corrosion in cracks, Doutoral Thesis, Department of Civil and Environmental Engineering, Division of Structural Engineering, Luleå University of Technology, Sweden; 2005.
- [35] prEN 12390-13. Testing hardened concrete – Part 13: Determination of secant modulus of elasticity in compression, Austrian Standards Institute/Österreichisches Normungsinstitut (ON), Vienna; 2012.
- [36] Rahmani T, Kiani B, Sami F, Fard B, Farnam Y, Shekarchizadeh M. Durability of glass, polypropylene and steel fiber reinforced concrete, Proceedings of XII DBMC - International Conference on Durability of Building Materials and Components, 12<sup>th</sup>–15<sup>th</sup> April 2011, Oporto-Portugal.
- [37] Rapoport J, Aldea C, Shah S, Ankenman B, Karr A. Permeability of cracked steel fiber reinforced concrete, Technical Report Number 115. USA: National Institute of Statistical Sciences; 2001.
- [38] RILEM CPC11.2, Absorption of water by concrete by capillarity, 2<sup>nd</sup> edition, RILEM Recommendations for the Testing and use of Construction Materials, E&FN SPON, Great Britain; 1994. p. 34–35.
- [39] RILEM TC 154-EMC. Electrochemical techniques for measuring metallic corrosion. *Mater Struct* 2004;37:623–43.
- [40] RILEM TC 162-TDF. Test and design methods for steel fibre reinforced concrete.  $\sigma$ - $\epsilon$ -design method. Final recommendation. *Mater Struct* 2003;36:560–7.
- [41] Roque R, Kim N, Kim B, Lopp G. Durability of Fiber-Reinforced Concrete in Florida Environments, Final Report, Project No.: 00050493, Department of Civil and Coastal Engineering, University of Florida, USA; 2009.
- [42] Sadeghi-Pouya H, Ganjian E, Claisse P, Muthuramalingam K. Corrosion durability of high performance steel fibre reinforced concrete, Proceedings of 3<sup>rd</sup> International Conference on Sustainable Construction Materials and Technologies, August 2013, Kyoto, Japan.
- [43] Sanchez M, Alonso M, Barragán B. Durability performance of Plain and Fiber Reinforced self-compacting concrete, PHI- Planta de Hormigón Internacional, No.2; 2009. p. 62–64.
- [44] Saojeng S, Weiting L. Effects of silica fume and steel fiber on chloride ion penetration and corrosion behavior of cement-based composites. *J Wuhan Univ Technol Mater Sci Ed* 2013;28(2).
- [45] Shi X, Xie N, Fortune K, Gong J. Durability of steel reinforced concrete in chloride environments: an overview. *Constr Build Mater* 2012;30:125–38.
- [46] Singh A, Singhal D. Permeability of steel fibre reinforced concrete influence of fibre parameters. *Proc Eng* 2011;14:2823–9.
- [47] Solgaard A, Kuter A, Edvardsen C, Stang H, Geiker M. Durability Aspects of Steel Fibre Reinforced Concrete in Civil Infrastructure, Proceedings of 2<sup>nd</sup> International Symposium on Service Life Design for Infrastructure, 4<sup>th</sup>–6<sup>th</sup> October 2010, Delft, The Netherlands.
- [48] Teruzzi T, Cadoni E, Frigeri G, Cangiano S, Plizzari G. Durability aspects of steel fibre reinforced concrete, Proc. BEFIB'2004 – 6<sup>th</sup> International RILEM Symposium on Fibre-Reinforced Concretes (FRC), 20<sup>th</sup>–22<sup>nd</sup> September 2004, Varenna, Italy. p. 625–634.
- [49] Tsai C, Li L, Chang C, Hwang C. Durability design and application of steel fiber reinforced concrete in Taiwan. *Arab J Sci Eng* 2009;34(1B).
- [50] Wang K, Jansen D, Shah S, Karr A. Permeability study of cracked concrete. *Cem Concr Res* 1997;27:381–93.
- [51] Yoon I. Chloride penetration through cracks in high-performance concrete and surface treatment system for crack healing, Hindawi Publishing Corporation. *Adv Mater Sci Eng* 2012;294571:8.
- [52] Vandewalle L et al. Test and design methods for steel fiber reinforced concrete. Recommendations for bending test. *Mater. Struct.* 2000;33(225):3–5.